

CERN-EP-2022-155
2022/08/05

CMS-TOP-21-014

Measurement of the $t\bar{t}$ charge asymmetry in events with highly Lorentz-boosted top quarks in pp collisions at $\sqrt{s} = 13$ TeV

The CMS Collaboration

Abstract

The measurement of the charge asymmetry in top quark pair events with highly Lorentz-boosted top quarks decaying to a single lepton and jets is presented. The analysis is performed using proton-proton collisions at $\sqrt{s} = 13$ TeV with the CMS detector at the LHC and corresponding to an integrated luminosity of 138 fb^{-1} . The selection is optimized for top quarks produced with large Lorentz boosts, resulting in nonisolated leptons and overlapping jets. The top quark charge asymmetry is measured for events with a $t\bar{t}$ invariant mass larger than 750 GeV and corrected for detector and acceptance effects using a binned maximum likelihood fit. The measured top quark charge asymmetry of $(0.69^{+0.65}_{-0.69})\%$ is in good agreement with the standard model prediction at next-to-next-to-leading order in quantum chromodynamic perturbation theory with next-to-leading-order electroweak corrections. The result is also presented for two invariant mass ranges, 750–900 and >900 GeV.

Submitted to Physics Letters B

arXiv:2208.02751v1 [hep-ex] 4 Aug 2022

1 Introduction

The vast majority of top quarks produced at hadron colliders are from $t\bar{t}$ pairs that originate from a $g\bar{t}t$ vertex via the strong interaction, where g is a gluon [1, 2]. The production of $t\bar{t}$ from proton-proton (pp) collisions at the LHC come from gluon fusion about 90% of the time, with $q\bar{q}$ annihilation making up the rest. At leading order, the standard model (SM) predicts that $t\bar{t}$ production from $q\bar{q}$ annihilation is forward-backward symmetric. However, higher-order SM effects result in a small ($\approx 6.6\%$) positive forward-backward asymmetry A_{FB} , such that the top quark (antiquark) is preferentially emitted in the direction of the incoming quark (antiquark) [3]. There is no asymmetry in the gluon fusion $t\bar{t}$ production that dominates at the LHC, but because valence quarks carry, on average, larger momentum than antiquarks (from the sea), the rapidity distribution of top quarks at the LHC is expected to be broader than that of top antiquarks [4, 5]. The $t\bar{t}$ charge asymmetry is defined as

$$A_C = \frac{N(\Delta|y| > 0) - N(\Delta|y| < 0)}{N(\Delta|y| > 0) + N(\Delta|y| < 0)}, \quad (1)$$

where $\Delta|y| = |y_t| - |y_{\bar{t}}|$ is the difference between the absolute value of the top quark and antiquark rapidities and N is the number of events. The value of A_C is expected to be about 1% in the SM for LHC [4].

Since the relative contribution of valence quarks increases at high momentum transfer [6], we expect that measuring A_C in a sample of $t\bar{t}$ events with highly Lorentz-boosted top quarks will lead to a more stringent probe of quantum chromodynamic (QCD) predictions and higher sensitivity to beyond-the-SM (BSM) physics processes that might alter the charge asymmetry [7]. Several models predict enhancements with respect to the SM prediction in the presence of new particles, including axigluons [8, 9], Z' bosons [10–12], W' bosons [9, 12, 13], scalar isodoublets [14], color triplet scalars [15, 16], and color sextet scalars [13, 14]. These models introduce new spin-0 and spin-1 particles in the interaction, modifying A_C by exchanging the new particles through interference terms and dedicated loops. Along with specific BSM models, deviations from the SM prediction can also be interpreted through an effective field theory approach in which new physics contributions are described via a fixed set of dimension-six operators added to the SM Lagrangian [17]. The ATLAS and CMS Collaborations have combined their inclusive and differential measurements of A_C [18] at two center-of-mass energies, obtaining $A_C = 0.005 \pm 0.007$ (stat) ± 0.006 (syst) and 0.0055 ± 0.0023 (stat) ± 0.0025 (syst) at 7 and 8 TeV, respectively. These combined measurements show good agreement with the respective SM predictions and uniquely restrict the phase space of possible BSM phenomena that would produce large asymmetries [13].

This Letter presents the first measurement of the $t\bar{t}$ charge asymmetry that uses pp collision data at $\sqrt{s} = 13$ TeV and optimizes the reconstruction of events with $t\bar{t}$ invariant mass ($M_{t\bar{t}}$) above 750 GeV. The kinematic requirements necessarily imply highly boosted top quarks. We target the single-lepton channel, in which both top quarks decay as $t \rightarrow bW$, with one W boson decaying leptonically ($W \rightarrow \ell\nu$, where ℓ is either a muon or electron), and the other hadronically ($W \rightarrow q\bar{q}'$). The highly boosted top quarks yield collimated decay products that are partially or fully merged. For the top quark decaying to a W boson that decays leptonically (called a top quark leptonic decay), this results in the lepton appearing as nonisolated because of its proximity to the b quark. Dedicated jet and lepton selection requirements at the trigger and offline levels [19] allow us to reconstruct the decay products of the boosted leptonically decaying top quarks without applying an isolation requirement on the leptons, while the QCD multijet background is controlled with topological requirements. The topology of the top quark decaying to a W boson that decays hadronically (called a top quark hadronic decay) depends

on the magnitude of its transverse momentum (p_T). At the high end of the p_T spectrum, the top quark decay products have angular distances between partons that can be smaller than the jet clustering distance parameter and are thus reconstructed as a single, large-radius jet. In contrast, at the low end of the p_T spectrum near the kinematic threshold, each parton is matched to a single jet. For intermediate p_T values, the partons from the hadronic W boson decay are merged into a single jet, but the b quark is reconstructed separately. All three topologies are considered in this analysis and are referred to as “boosted”, “semiresolved”, and “resolved” for the high, intermediate, and low p_T regions, respectively. Tabulated results are provided in the HEPData record for this analysis [20].

2 The CMS detector and object reconstruction

The central feature of the CMS apparatus is a superconducting solenoid of 6 m internal diameter, providing a magnetic field of 3.8 T. Within the solenoid volume are a silicon pixel and strip tracker, a lead tungstate crystal electromagnetic calorimeter, and a brass and scintillator hadron calorimeter, each composed of a barrel and two endcap sections. Forward calorimeters extend the pseudorapidity (η) coverage provided by the barrel and endcap detectors. Muons are measured in gas-ionization detectors embedded in the steel flux-return yoke outside the solenoid. Events of interest are selected using a two-tiered trigger system [21, 22]. A more detailed description of the CMS detector, together with a definition of the coordinate system used and the relevant kinematic variables, can be found in Ref. [23].

The offline event reconstruction is based on a particle-flow (PF) algorithm [24], which combines information from each subdetector to identify electrons, photons, and charged or neutral hadrons. To recover inefficiencies observed in data for very high p_T PF muons, we use muons that are reconstructed first in the muon system and then fitted to tracks [25]. The primary vertex is taken to be the vertex corresponding to the hardest scattering in the event, evaluated using tracking information alone, as described in Section 9.4.1 of Ref. [26]. Charged hadrons associated with other vertices are removed from further consideration. The remaining PF candidates are clustered into jets using the anti- k_T algorithm [27, 28] with a distance parameter of 0.4 (called AK4 jets). The same PF candidates are used to build large-radius (AK8) jets using a distance parameter of 0.8 and the pileup per particle identification algorithm [29, 30]. Any AK4 jet with $\Delta R = \sqrt{(\Delta\eta)^2 + (\Delta\phi)^2} < 0.8$ from the closest AK8 jet, where ϕ is the azimuthal angle, is discarded from the event. The total jet \vec{p}_T is given by the sum of the \vec{p}_T of its constituents. If a lepton is found within $\Delta R < 0.4$ of an AK4 jet or < 0.8 of an AK8 jet, its four-momentum is subtracted from that jet [19]. The missing transverse momentum vector \vec{p}_T^{miss} is computed as the negative vector sum of the transverse momenta of all the PF candidates in an event, and its magnitude is denoted as p_T^{miss} [31]. Corrections are applied to improve the jet energy scale and resolution, and the \vec{p}_T^{miss} is modified to account for these corrections [32, 33].

Specialized techniques use AK8 jets and jet substructure information [34], including “soft-drop clustering” [35] and “N-subjettiness” [36], to identify the hadronic decay of boosted top quarks, following the techniques detailed in Ref. [19]. Two exclusive categories are considered: hadronically decaying top quarks (t tag) in which the three partons are merged into a single AK8 jet, and hadronically decaying W bosons (W tag) in which the two partons from the W boson are merged into a single AK8 jet, but the bottom quark is reconstructed as a separate AK4 jet. The identification of jets originating from the decay of b hadrons (b tag) employs a deep neural network multi-classification algorithm (DEEPJET [37]) that relies on information from the tracker and the calorimeters [38]. The b tagging algorithm is applied to each AK4 jet j with $p_T^j > 50$ GeV

and $|\eta^j| < 2.4$. The t and W tagging algorithms are applied to AK8 jets with $p_T^j > 400$ GeV and $|\eta^j| < 2.4$. The algorithms are tuned for low misidentification rates and have efficiencies greater than 80%.

3 Collider data and simulated samples

We analyze data collected by the CMS detector during Run 2 (2016–2018) and corresponding to a total integrated luminosity of up to 138 fb^{-1} [39–41]. Events in the muon channel ($\mu + \text{jets}$) are selected with a single-muon trigger that requires $p_T^\mu > 50$ GeV. Events in the electron channel ($e + \text{jets}$) are selected by either a single-electron trigger with $p_T^e > 115$ GeV or a trigger requiring one electron with $p_T^e > 50$ GeV and one jet with $p_T^j > 165$ GeV [19]. As the $e + \text{jets}$ trigger was not available during the early running period in 2017, the integrated luminosity available for the 2017 $e + \text{jets}$ channel is reduced by 5 fb^{-1} .

In the offline reconstruction, we select events for the $\mu + \text{jets}$ ($e + \text{jets}$) channel that contain exactly one muon with $p_T^\mu > 55$ GeV and $|\eta^\mu| < 2.4$ (one electron with $p_T^e > 80$ GeV and $|\eta^e| < 2.5$) and at least two jets, j_1 and j_2 , with $p_T^{j_1} > 150$ (185) GeV, $p_T^{j_2} > 50$ GeV, and $|\eta^{j_{1,2}}| < 2.4$. To preserve the identification efficiency of $t\bar{t}$ decay products in the highly boosted topology, no isolation requirement is imposed on the leptons at either the trigger or offline level. To reduce the background from QCD multijet events, we apply a two-dimensional (2D) selection that requires leptons to satisfy either the condition $\Delta R_{\min}(\ell, j) > 0.4$ or $p_{T,\text{rel}}(\ell, j) > 25$ GeV, where $\Delta R_{\min}(\ell, j)$ is the angular separation between the lepton and the closest AK4 jet, and $p_{T,\text{rel}}(\ell, j)$ is the transverse momentum of the lepton with respect to the axis of the nearest AK4 jet [19]. Finally, events need to satisfy $p_T^{\text{miss}} > 50$ GeV and $p_T^{\text{miss}} + p_T^\mu > 150$ GeV ($p_T^{\text{miss}} > 120$ GeV) in the $\mu + \text{jets}$ ($e + \text{jets}$) channel. The larger value of the $e + \text{jets}$ p_T^{miss} requirement efficiently reduces the larger QCD multijet background in this channel and obviates the need for a separate requirement on $p_T^{\text{miss}} + p_T^e$. To suppress the contribution from the $W + \text{jets}$ background, at least one of the AK4 jets must be b tagged.

Monte Carlo (MC) samples for the $t\bar{t}$ [42] and single top quark (ST) processes are produced with the next-to-leading-order (NLO) POWHEG [43] generator. Simulated $W + \text{jets}$, Drell–Yan (DY) $Z/\gamma + \text{jets}$, and QCD multijet processes are generated with MADGRAPH5_aMC@NLO [44] at NLO. All samples are interfaced to PYTHIA8 [45] for parton showering with the CP5 tune [46]. Vector boson pair (diboson) events are simulated with PYTHIA8. The NNPDF 3.0 (2016) and NNPDF 3.1 (2017 and 2018) parton distribution functions (PDFs) [47] are used for all samples and include the simulation of additional inelastic pp interactions (pileup) within the same or nearby bunch crossings. Small corrections are applied to all MC samples to improve the agreement with the observed data, derived from data control samples that are independent of the candidate selection. In particular, the transverse momentum of the top quarks at the generator level is corrected to match the distribution measured in data [48].

4 Reconstruction of the top quark pair events

The $t\bar{t}$ system is reconstructed by assigning the four-vectors of the final-state objects to either the leptonic (t_ℓ) or hadronic (t_h) leg of the $t\bar{t}$ decay. The events are separated into the three topologies discussed earlier based on the presence of t- or W-tagged jets: boosted contains events with one t tag and no W tag; semiresolved contains events with one W tag and no t tag; and resolved contains the rest of the events that have no t and no W tag. Events with more than one t or W tag are discarded. For events with a t tag, the t-tagged jet is taken as the t_h

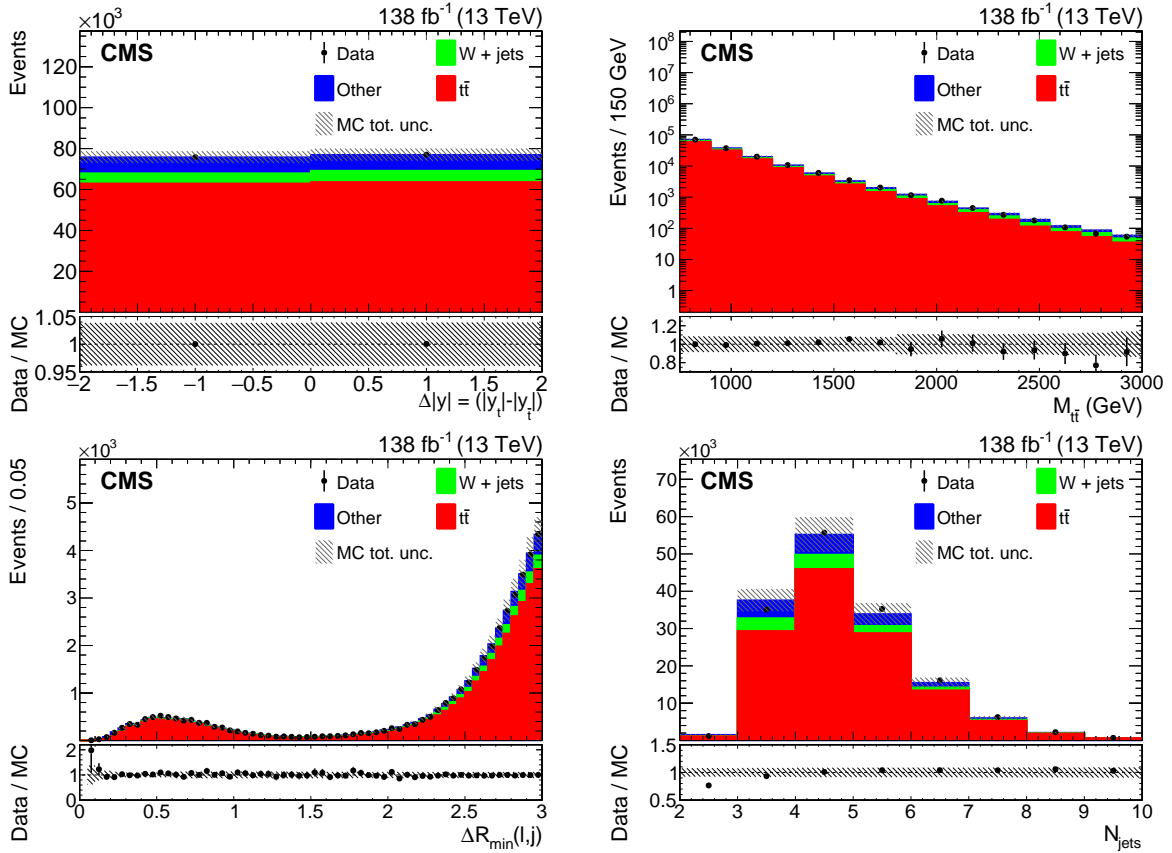


Figure 1: Comparison between data and MC simulation for kinematic distributions based on events in the signal candidate sample (described in Section 6): $\Delta|y|$ (upper left), reconstructed $M_{t\bar{t}}$ (upper right), distance between the lepton and the closest AK4 jet $\Delta R_{\min}(\ell, j)$ (lower left), and the number of AK4 jets (lower right). The vertical bars on the points show the statistical uncertainty in the data. The shaded bands represent the total uncertainty in the MC predictions (described in Section 5). The lower panels give the ratio of the data to the sum of the MC predictions.

and only AK4 jets with $\Delta R > 0.8$ from the t_h are considered as candidates for the t_ℓ . For events with a W tag, the W-tagged jet is assigned to the t_h . The AK4 jets with $\Delta R > 0.8$ from the W tag can be assigned to either the t_ℓ or the t_h . For events with neither a t tag nor a W tag, all possible assignments of AK4 jets are considered for both the t_ℓ and the t_h . Even though each event includes at least one b-tagged jet, the b tagging information for individual jets is not used in this process. The longitudinal component of the neutrino momentum is inferred by constraining the invariant mass of the lepton plus neutrino system to the W boson mass [49].

For each event, one $t\bar{t}$ hypothesis is selected based on the smallest value of the χ^2 variable that minimizes the difference between the reconstructed t_ℓ and t_h masses and the top quark mass determined from simulation for each topology with the procedure in Ref. [19]. Because background processes typically result in large values of χ^2 , only events with $\chi^2 < 30$ are retained. Finally, our signal candidate sample is defined as those events with $t\bar{t}$ invariant mass greater than 750 GeV. Figure 1 shows comparisons between data and MC simulation for kinematic distributions based on events in the candidate sample. The boosted nature of the top quarks in the events becomes evident: the $M_{t\bar{t}}$ range extends to multi-TeV values, events with two and three AK4 jets originating from the collimated top quark decay products are reconstructed, and events with leptons closer to the nearest jet axis than the jet size are retained. Good agreement

between data and prediction is observed in all cases.

5 Systematic uncertainties

Systematic uncertainties from numerous sources can affect the normalization and the shape of the distributions of physical observables in both signal and background samples. The systematic uncertainties affecting only the normalization come from the SM theoretical cross section values for each process and the luminosity normalization. All MC samples are normalized according to their respective SM cross section values and assigned a rate uncertainty of 30% for background processes and 5% for the $t\bar{t}$ signal [50]. Additionally, uncertainties in the integrated luminosity vary per year: 2.5, 2.3, and 1.2% for 2018 [41], 2017 [40], and 2016 [39], respectively, and include both correlated and uncorrelated components across the three years, while the overall uncertainty for the 2016–2018 period is 1.6%.

All other systematic uncertainties affect both the normalization and shape of the MC distributions. Uncertainties from experimental sources are applied to both signal and background samples. All MC samples are reweighted to match the pileup distribution in data, which is generated by using the instantaneous luminosity per bunch crossing for each luminosity section, with a total inelastic cross section of 69.2 mb; an uncertainty of 4.6% is applied to this value [51]. All muons and electrons in the simulated samples have uncertainties associated with the high-level trigger (HLT), reconstruction (reco), and identification (ID). The uncertainty associated with the possible misidentification of the sign of the lepton electric charge is negligible. These uncertainties are uncorrelated across lepton flavors but correlated across years and are parameterized as a function of the p_T and η of the leptons. There is a uniform uncertainty in the efficiency of the 2D selection that rejects QCD background, and this is uncorrelated across lepton flavors and years. Uncertainties in the jet energy corrections (JEC) and resolution (JER) are parameterized in terms of the jet p_T and η and considered correlated across years. The uncertainties in the tagging scale factors are parameterized as a function of the jet p_T . The uncertainties in t and W tagging are 100% correlated across years, but the uncertainty in b tagging has both correlated and uncorrelated components [52]. There are different scale factors to account for the cases when the tagging algorithms incorrectly identify (mistag) some jets, so a separate mistagging uncertainty is also assigned.

In addition to the experimental sources, we consider uncertainties affecting the MC simulations. The uncertainty from the choice of PDF is estimated by taking the difference between using versions 3.0 and 3.1 of the NNPDF sets according to the procedure described in Ref. [53]. Renormalization (μ_R) and factorization (μ_F) scales at the matrix element level are varied by a factor of 2 or 0.5 to take into account the effect of higher-order corrections in the $t\bar{t}$ and $W + \text{jets}$ simulations. The matrix element and parton shower matching scale (h_{damp}) regulates the high- p_T radiation by damping real emissions from the POWHEG generator; this effect is only taken into account for $t\bar{t}$ and evaluated using independent simulated samples. Uncertainties related to the modeling of initial- and final-state radiation (ISR and FSR) in the parton shower are determined by varying the strong coupling constant α_s at the scale Q^2 for the $t\bar{t}$ samples. Finally, an uncertainty in the correction to the top quark p_T is evaluated as a one-sided variation computed from the difference between the top quark p_T distribution with and without the correction [48]. For all these uncertainties, those originating from the same source are considered as 100% correlated between channels and those arising from different sources are considered to be 100% uncorrelated.

6 Unfolded results

The top quark charge asymmetry is obtained by performing a simultaneous binned maximum likelihood fit to data in all bins and categories of the signal candidate sample that will be described below. Statistical uncertainties due to the MC sample size are treated separately in each bin with the Barlow–Beeston-lite approach [54]. Each source of systematic uncertainty is included in the likelihood as a unique nuisance parameter. For contributions that apply to multiple analysis channels, the nuisance parameters are fully correlated, allowing better constraints to be placed on the systematic uncertainties. For a given channel k in our analysis, the channel likelihood function \mathcal{L}_k is defined as:

$$\mathcal{L}_k = \prod_{j=1}^{N_{\text{reco}}} P \left(n_j; \sum_{i=1}^{N_{\text{gen}}} A_{ji}(\vec{\delta}_u) \mu_i + b_j \right) N(\vec{\delta}_u), \quad (2)$$

where

- $P(n; \mu)$ represents the Poisson probability of observing n events when μ are expected.
- The index i runs over the number of bins at generator level (N_{gen}), and the index j runs over the number of bins at reconstruction level (N_{reco}). In this analysis, we use two bins corresponding to the positive and negative difference between the absolute value of the top quark and antiquark rapidities $\Delta|y|$. Correspondingly, N_{reco} and N_{gen} are both set equal to 2.
- The response matrix A_{ji} gives the probability for an event produced in bin i to be measured in bin j .
- n_j corresponds to the number of data events in bin j .
- b_j represents the number of background events predicted in bin j .
- $N(\vec{\delta}_u)$ represents the priors for the nuisance parameters corresponding to individual uncertainty sources δ_u . Normalization uncertainties are assigned to a log-normal distribution, all other uncertainties have a normal distribution prior.

Each analysis channel is defined by a range of $M_{t\bar{t}}$ values and a specific year and lepton flavor. The total likelihood is given by the product of the individual likelihoods from Eq. (2), with the index k running over all 12 channels: two lepton flavors ($\mu + \text{jets}$ and $e + \text{jets}$), 3 years (2018, 2017, and 2016), and two mass regions ($750 < M_{t\bar{t}} < 900 \text{ GeV}$ and $M_{t\bar{t}} > 900 \text{ GeV}$). This unfolding approach also has the advantage that the background contributions are constrained by the fit, resulting in smaller systematic uncertainties than those obtained with a direct background subtraction.

Table 1 shows the signal and background yields in our final candidate sample after the likelihood fit, separated into the two mass regions. The contributions to our candidate sample from background processes (ST, $W + \text{jets}$, DY, and QCD multijet) are taken from simulation and their normalization allowed to change during the likelihood fit. The diboson background yield is negligible and therefore omitted from the table. The higher p_T thresholds on the lepton and highest p_T jet in the electron channel result in significantly reduced signal acceptance compared to the muon channel, as evident in the yields. Figure 2 shows $\Delta|y|$ for each of these 12 channels both before and after the likelihood normalization. As can be observed, the likelihood fit reduces the total uncertainty significantly and improves the agreement between data and the MC prediction.

Table 1: The signal event yields in data and MC simulations after the likelihood fit for each of the 12 channels (μ + jets, e + jets, 3 years; and two mass regions). The uncertainties in the MC predictions include both statistical and systematic components.

Process	μ (2018)	μ (2017)	μ (2016)	e (2018)	e (2017)	e (2016)
$750 < M_{t\bar{t}} < 900 \text{ GeV}$						
$t\bar{t}$	$22\,230 \pm 1950$	$16\,430 \pm 1400$	$10\,370 \pm 970$	4590 ± 450	2950 ± 260	2560 ± 240
ST	1620 ± 150	2150 ± 190	910 ± 80	410 ± 30	510 ± 40	290 ± 30
W + jets	970 ± 110	1150 ± 120	1250 ± 270	240 ± 30	220 ± 30	320 ± 70
DY	90 ± 20	40 ± 10	50 ± 10	15 ± 3	6 ± 1	10 ± 2
QCD multijet	410 ± 100	270 ± 60	180 ± 40	6 ± 2	2 ± 1	0 ± 0
Total	$25\,310 \pm 1960$	$20\,050 \pm 1400$	$12\,770 \pm 1000$	5270 ± 450	3690 ± 260	3180 ± 250
Data	25417	20052	12735	5219	3674	3127
$M_{t\bar{t}} > 900 \text{ GeV}$						
$t\bar{t}$	$23\,340 \pm 2270$	$17\,120 \pm 1640$	$10\,700 \pm 1060$	7140 ± 740	4880 ± 490	4110 ± 430
ST	1670 ± 140	2020 ± 170	920 ± 80	610 ± 60	690 ± 60	420 ± 40
W + jets	1450 ± 170	1330 ± 160	1970 ± 450	520 ± 60	440 ± 50	740 ± 160
DY	110 ± 20	60 ± 10	70 ± 10	30 ± 6	14 ± 3	20 ± 4
QCD multijet	860 ± 120	810 ± 130	470 ± 70	10 ± 3	30 ± 9	40 ± 10
Total	$27\,400 \pm 2280$	$21\,350 \pm 1660$	$14\,130 \pm 1160$	8320 ± 750	6050 ± 500	5330 ± 460
Data	27298	21358	14157	8361	6066	5385

Combinations of subsets of these channels are also possible and allow us to obtain results for the two mass regions separately. In all cases, the unfolding performs a multi-dimensional maximum likelihood fit of the simulation to the observed data and returns two measured parameters. One way to measure A_C^{fid} , the top quark charge asymmetry in the fiducial phase space, is to fit for r_{pos} and r_{neg} , the signal strengths that scale the contribution of events with $\Delta|y| > 0$ and < 0 , respectively, and then use Eq. (1) to determine A_C^{fid} . Instead, we fit for r_{neg} and A_C^{fid} directly to ensure that the uncertainty in A_C^{fid} is correctly estimated.

Table 2 and Fig. 3 (left) summarize the A_C^{fid} values for two different invariant mass regions, along with their statistical and systematic uncertainties. The theoretical predictions include the next-to-NLO (NNLO) QCD and NLO EW corrections from Ref. [4], and are obtained by setting the observed quantities to their expected values (“Asimov data”). As can be observed, the measured A_C^{fid} is consistent, within the uncertainty, with the expectations.

The unfolded charge asymmetry at parton level A_C is obtained after correcting for the product of the acceptance determined at generator level times the event selection efficiency ($\alpha\varepsilon$). Specifically, the number of unfolded signal events in each channel is divided by the corresponding $\alpha\varepsilon$ to correct from the fiducial phase space of that channel to the full phase space, which is common to all 12 channels. The uncertainty in the acceptance arising from theoretical sources in the $t\bar{t}$ generation is several orders of magnitude smaller than the dominant systematic uncertainty and therefore neglected.

Table 2 and Fig. 3 (right) show the measured top quark charge asymmetry after unfolding to parton level in the full phase space, compared with the theoretical prediction at NNLO QCD and NLO EW corrections from Ref. [4]. Good agreement between the data and the MC prediction is observed. Figure 4 shows the ± 1 standard deviation (σ) impacts of the systematic uncertainties in the A_C measurements for the full signal sample.

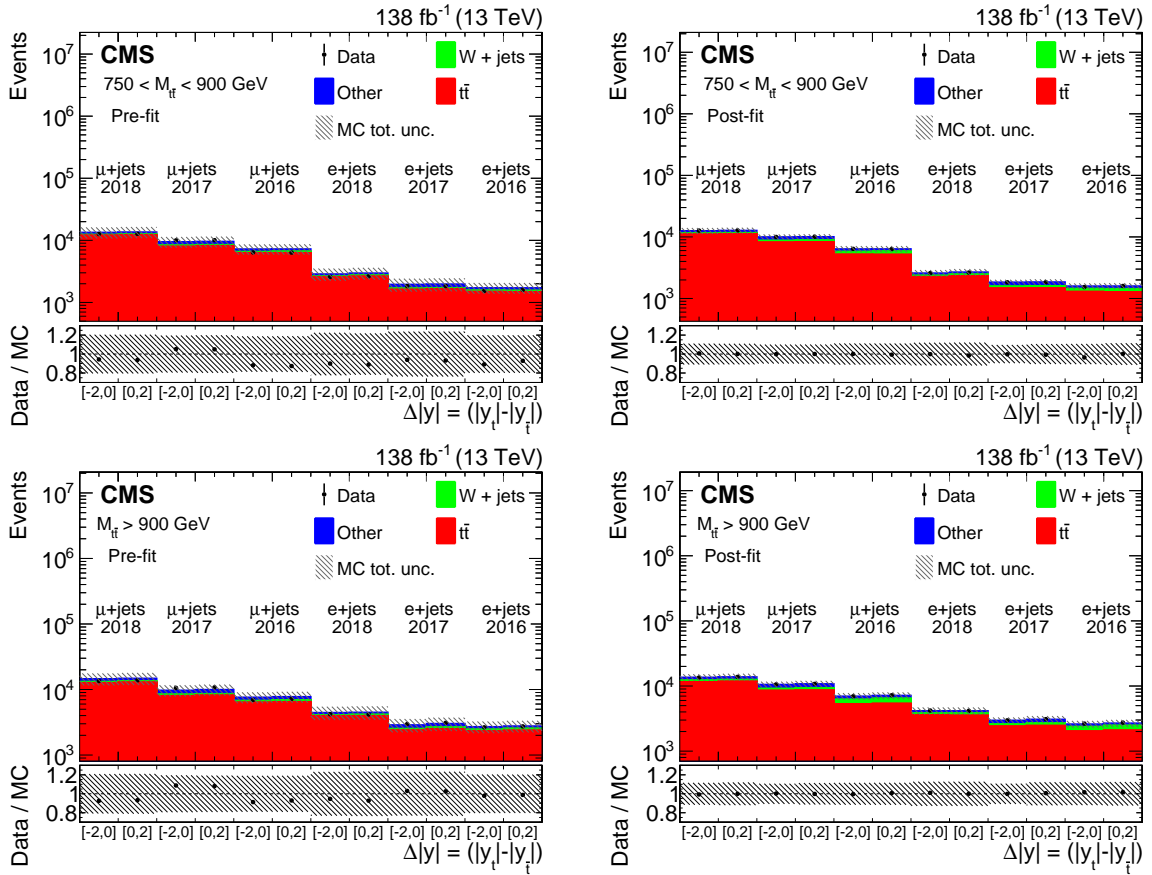


Figure 2: Comparison between data and MC simulation for $\Delta|y|$ for each of the 12 analysis channels, both before (left) and after (right) the likelihood normalization. The plots in the upper row correspond to $750 < M_{t\bar{t}} < 900$ GeV, and the plots in the lower row to $M_{t\bar{t}} > 900$ GeV. The vertical bars on the points represent the statistical uncertainties in the data and the shaded bands give the combined MC statistical and systematic uncertainties. The lower panels display the ratio of the data yields to the sum of the MC predictions.

Table 2: Measured unfolded charge asymmetry in the fiducial phase space (upper rows) and the full phase space (lower rows) shown for individual channels compared with the theoretical prediction from MC. Results are shown for events with $M_{t\bar{t}} > 750$ GeV and for two invariant mass ranges, 750–900 and >900 GeV. The statistical (stat) and systematic (syst) uncertainties in the data, the MC statistical uncertainty (MC stat), and the total uncertainty in the measured values (Total) are also shown. All values are in percent.

$M_{t\bar{t}}$ (GeV)	A_C (%)					Theory
	Measured	Stat	Syst	MC stat	Total	
Fiducial phase space (A_C^{fid})						
> 750	0.22	± 0.44	$+0.34$ -0.43	± 0.32	$+0.64$ -0.69	0.72 -0.61
750 – 900	0.39	$+0.66$ -0.65	$+0.39$ -0.56	$+0.43$ -0.44	$+0.88$ -0.96	0.60 -0.91
> 900	1.18	± 0.58	$+0.55$ -0.75	± 0.41	$+0.90$ -1.03	0.83 -0.82
Full phase space (A_C)						
> 750	0.69	± 0.44	$+0.34$ -0.42	± 0.32	$+0.65$ -0.69	0.94 -0.07
750 – 900	2.43	± 0.65	$+0.29$ -0.64	$+0.45$ -0.43	$+0.84$ -1.01	0.87 -0.08
> 900	0.37	± 0.58	$+0.55$ -0.72	$+0.41$ -0.40	$+0.90$ -1.01	1.01 $+0.06$ -0.07

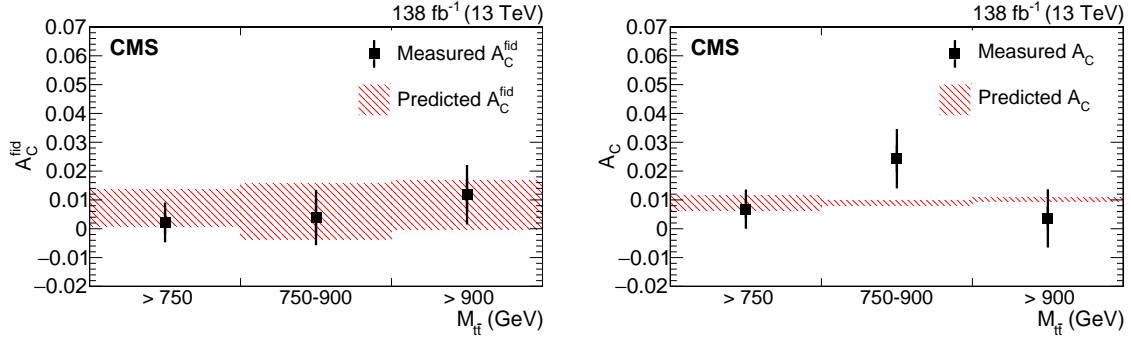


Figure 3: Measured A_C^{fid} (left) and measured A_C in the full phase space (right) presented in different mass regions after combining the $\mu + \text{jets}$ and $e + \text{jets}$ channels. The vertical bars represent the total uncertainties, with the inner tick mark indicating the statistical uncertainty in the observed data. The measured values are compared to the theoretical prediction, including NNLO QCD and NLO EW corrections from Ref. [4]. The theoretical prediction in the fiducial region is obtained by fitting Asimov data that passed the signal candidate selection described in Sections 3 and 4.

7 Summary

The first measurement of the charge asymmetry in $t\bar{t}$ events with highly boosted top quarks produced in proton-proton collisions at $\sqrt{s} = 13$ TeV is presented based on 138 fb^{-1} of data collected by the CMS experiment at the LHC. The selection is optimized for top quarks produced with high Lorentz boosts that yield collimated decay products that are partially or fully merged and can result in nonisolated leptons and overlapping jets. The measured top quark charge asymmetry (A_C) is corrected for detector and acceptance effects using a binned maximum likelihood fit.

This is the first measurement to use 13 TeV data and a binned maximum likelihood unfolding

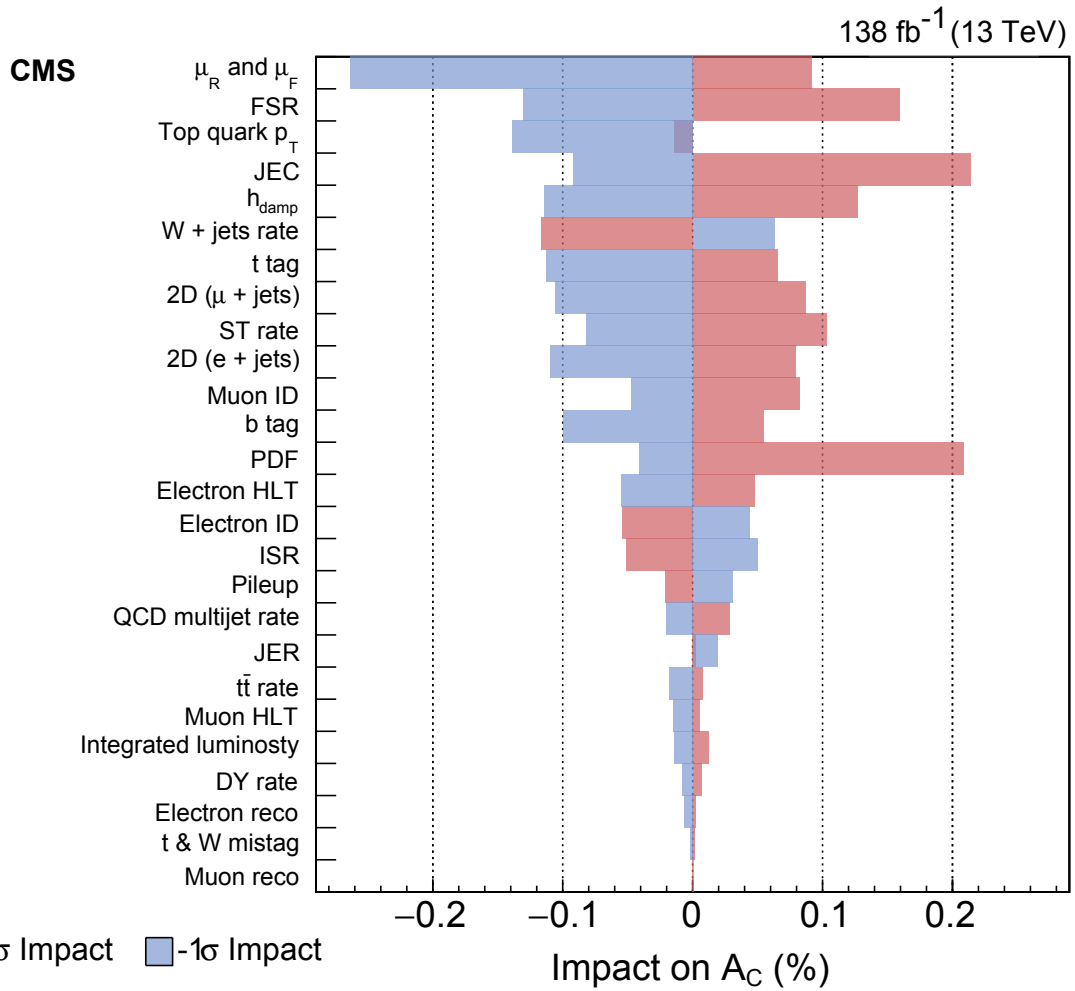


Figure 4: The ± 1 standard deviation (σ) impacts of the nuisance parameters corresponding to the systematic uncertainties in the full phase space A_C measurement for $M_{t\bar{t}} > 750$ GeV. The red and blue bars show the effect on the unfolded A_C values for up and down variations of the systematic uncertainty. The MC statistical uncertainties are omitted here.

technique to measure A_C directly at parton level in the full phase space. In addition, it is the first result that focuses exclusively on the highly Lorentz-boosted regime, using dedicated reconstruction techniques for the hadronically and leptonically decaying top quarks at both the trigger and offline stages. Since the relative contribution of valence quarks increases at high momentum transfer, A_C is especially sensitive to beyond the standard model processes in this highly boosted phase space.

The resulting unfolded charge asymmetry for $t\bar{t}$ events with invariant masses satisfying $M_{t\bar{t}} > 750$ GeV, corrected to the full phase space, is $(0.69_{-0.69}^{+0.65})\%$, where the uncertainty includes both statistical and systematic components. The corresponding theoretical prediction at next-to-next-to-leading order in QCD perturbation theory with next-to-leading-order electroweak corrections from Ref. [4] is $(0.94_{-0.07}^{+0.05})\%$. Good agreement between the measurement and the most precise standard model prediction is thus observed. The result demonstrates that top quark properties can be precisely measured in the highly boosted topology.

References

- [1] M. Czakon, P. Fiedler, and A. Mitov, "Total top-quark pair-production cross section at hadron colliders through $\mathcal{O}(\alpha_s^4)$ ", *Phys. Rev. Lett.* **110** (2013) 252004, doi:10.1103/PhysRevLett.110.252004, arXiv:1303.6254.
- [2] S. Catani et al., "Top-quark pair production at the LHC: Fully differential QCD predictions at NNLO", *JHEP* **07** (2019) 100, doi:10.1007/JHEP07(2019)100, arXiv:1906.06535.
- [3] M. Czakon, P. Fiedler, and A. Mitov, "Resolving the Tevatron top quark forward-backward asymmetry puzzle: Fully differential next-to-next-to-leading-order calculation", *Phys. Rev. Lett.* **115** (2015) 052001, doi:10.1103/physrevlett.115.052001, arXiv:1411.3007.
- [4] M. Czakon et al., "Top-quark charge asymmetry at the LHC and Tevatron through NNLO QCD and NLO EW", *Phys. Rev. D* **98** (2018) 014003, doi:10.1103/physrevd.98.014003, arXiv:1711.03945.
- [5] M. Czakon, D. Heymes, and A. Mitov, "High-precision differential predictions for top-quark pairs at the LHC", *Phys. Rev. Lett.* **116** (2016) 082003, doi:10.1103/physrevlett.116.082003, arXiv:1511.00549.
- [6] J. Rojo et al., "The PDF4LHC report on PDFs and LHC data: results from Run I and preparation for Run II", *J. Phys. G* **42** (2015) 103103, doi:10.1088/0954-3899/42/10/103103, arXiv:1507.00556.
- [7] J. A. Aguilar-Saavedra, A. Juste, and F. Rubbo, "Boosting the $t\bar{t}$ charge asymmetry", *Phys. Lett. B* **707** (2012) 92, doi:10.1016/j.physletb.2011.12.007, arXiv:1109.3710.
- [8] O. Antunano, J. H. Kuhn, and G. Rodrigo, "Top quarks, axigluons and charge asymmetries at hadron colliders", *Phys. Rev. D* **77** (2008) 014003, doi:10.1103/PhysRevD.77.014003, arXiv:0709.1652.
- [9] P. H. Frampton, J. Shu, and K. Wang, "Axigluon as possible explanation for $p\bar{p} \rightarrow t\bar{t}$ forward-backward asymmetry", *Phys. Lett. B* **683** (2010) 294, doi:10.1016/j.physletb.2009.12.043, arXiv:0911.2955.

-
- [10] J. L. Rosner, “Prominent decay modes of a leptophobic Z' ”, *Phys. Lett. B* **387** (1996) 113, doi:10.1016/0370-2693(96)01022-2, arXiv:hep-ph/9607207.
- [11] P. Ferrario and G. Rodrigo, “Massive color-octet bosons and the charge asymmetries of top quarks at hadron colliders”, *Phys. Rev. D* **78** (2008) 094018, doi:10.1103/physrevd.78.094018, arXiv:0809.3354.
- [12] P. Ferrario and G. Rodrigo, “Constraining heavy colored resonances from top-antitop quark events”, *Phys. Rev. D* **80** (2009) 051701, doi:10.1103/PhysRevD.80.051701, arXiv:0906.5541.
- [13] J. A. Aguilar-Saavedra and M. Perez-Victoria, “Asymmetries in $t\bar{t}$ production: LHC versus Tevatron”, *Phys. Rev. D* **84** (2011) 115013, doi:10.1103/PhysRevD.84.115013, arXiv:1105.4606.
- [14] J. A. Aguilar-Saavedra and M. Perez-Victoria, “Simple models for the top asymmetry: Constraints and predictions”, *JHEP* **09** (2011) 097, doi:10.1007/JHEP09(2011)097, arXiv:1107.0841.
- [15] R. Benbrik, C.-H. Chen, and M. El Kacimi, “Colored bosons on top FBA and angular cross section for $t\bar{t}$ production”, *Phys. Lett. B* **725** (2013) 372, doi:10.1016/j.physletb.2013.07.057, arXiv:1304.2273.
- [16] D.-W. Jung, P. Ko, J. S. Lee, and S.-h. Nam, “Model independent analysis of the forward-backward asymmetry of top quark production at the Tevatron”, *Phys. Lett. B* **691** (2010) 238, doi:10.1016/j.physletb.2010.06.040, arXiv:0912.1105.
- [17] C. Zhang and S. Willenbrock, “Effective-field-theory approach to top-quark production and decay”, *Phys. Rev. D* **83** (2011) 034006, doi:10.1103/PhysRevD.83.034006, arXiv:1008.3869.
- [18] ATLAS and CMS Collaborations, “Combination of inclusive and differential $t\bar{t}$ charge asymmetry measurements using ATLAS and CMS data at $\sqrt{s} = 7$ and 8 TeV”, *JHEP* **04** (2018) 033, doi:10.1007/JHEP04(2018)033, arXiv:1709.05327.
- [19] CMS Collaboration, “Search for resonant $t\bar{t}$ production in proton-proton collisions at $\sqrt{s} = 13$ TeV”, *JHEP* **04** (2019) 031, doi:10.1007/JHEP04(2019)031, arXiv:1810.05905.
- [20] HEPData record for this analysis, 2022. doi:10.17182/hepdata.127992.
- [21] CMS Collaboration, “Performance of the CMS Level-1 trigger in proton-proton collisions at $\sqrt{s} = 13$ TeV”, *JINST* **15** (2020) P10017, doi:10.1088/1748-0221/15/10/P10017, arXiv:2006.10165.
- [22] CMS Collaboration, “The CMS trigger system”, *JINST* **12** (2017) P01020, doi:10.1088/1748-0221/12/01/P01020, arXiv:1609.02366.
- [23] CMS Collaboration, “The CMS experiment at the CERN LHC”, *JINST* **3** (2008) S08004, doi:10.1088/1748-0221/3/08/S08004.
- [24] CMS Collaboration, “Particle-flow reconstruction and global event description with the CMS detector”, *JINST* **12** (2017) P10003, doi:10.1088/1748-0221/12/10/P10003, arXiv:1706.04965.

- [25] CMS Collaboration, “Description and performance of track and primary-vertex reconstruction with the CMS tracker”, *JINST* **9** (2014) P10009, doi:10.1088/1748-0221/9/10/P10009, arXiv:1405.6569.
- [26] CMS Collaboration, “Technical proposal for the Phase-II upgrade of the Compact Muon Solenoid”, CMS Technical Proposal CERN-LHCC-2015-010, CMS-TDR-15-02, 2015.
- [27] M. Cacciari, G. P. Salam, and G. Soyez, “The anti- k_T jet clustering algorithm”, *JHEP* **04** (2008) 063, doi:10.1088/1126-6708/2008/04/063, arXiv:0802.1189.
- [28] M. Cacciari, G. P. Salam, and G. Soyez, “FastJet user manual”, *Eur. Phys. J. C* **72** (2012) 1896, doi:10.1140/epjc/s10052-012-1896-2, arXiv:1111.6097.
- [29] D. Bertolini, P. Harris, M. Low, and N. Tran, “Pileup per particle identification”, *JHEP* **10** (2014) 059, doi:10.1007/JHEP10(2014)059, arXiv:1407.6013.
- [30] CMS Collaboration, “Pileup mitigation at CMS in 13 TeV data”, *JINST* **15** (2020) P09018, doi:10.1088/1748-0221/15/09/P09018, arXiv:2003.00503.
- [31] CMS Collaboration, “Performance of missing transverse momentum reconstruction in proton-proton collisions at $\sqrt{s} = 13$ TeV using the CMS detector”, *JINST* **14** (2019) P07004, doi:10.1088/1748-0221/14/07/P07004, arXiv:1903.06078.
- [32] CMS Collaboration, “Determination of jet energy calibration and transverse momentum resolution in CMS”, *JINST* **6** (2011) P11002, doi:10.1088/1748-0221/6/11/P11002, arXiv:1107.4277.
- [33] CMS Collaboration, “Jet energy scale and resolution in the CMS experiment in pp collisions at 8 TeV”, *JINST* **12** (2017) P02014, doi:10.1088/1748-0221/12/02/P02014, arXiv:1607.03663.
- [34] CMS Collaboration, “Identification of heavy, energetic, hadronically decaying particles using machine-learning techniques”, *JINST* **15** (2020) P06005, doi:10.1088/1748-0221/15/06/P06005, arXiv:2004.08262.
- [35] A. J. Larkoski, S. Marzani, G. Soyez, and J. Thaler, “Soft drop”, *JHEP* **05** (2014) 146, doi:10.1007/JHEP05(2014)146, arXiv:1402.2657.
- [36] J. Thaler and K. Van Tilburg, “Identifying boosted objects with N-subjettiness”, *JHEP* **03** (2011) 015, doi:10.1007/JHEP03(2011)015, arXiv:1011.2268.
- [37] CMS Collaboration, “Identification of heavy-flavour jets with the CMS detector in pp collisions at 13 TeV”, *JINST* **13** (2018) P05011, doi:10.1088/1748-0221/13/05/P05011, arXiv:1712.07158.
- [38] E. Bols et al., “Jet flavour classification using DeepJet”, *JINST* **15** (2020) P12012, doi:10.1088/1748-0221/15/12/P12012, arXiv:2008.10519.
- [39] CMS Collaboration, “Precision luminosity measurement in proton-proton collisions at $\sqrt{s} = 13$ TeV in 2015 and 2016 at CMS”, *Eur. Phys. J. C* **81** (2021) 800, doi:10.1140/epjc/s10052-021-09538-2, arXiv:2104.01927.
- [40] CMS Collaboration, “CMS luminosity measurement for the 2017 data-taking period at $\sqrt{s} = 13$ TeV”, CMS Physics Analysis Summary CMS-PAS-LUM-17-004, 2018.

-
- [41] CMS Collaboration, “CMS luminosity measurement for the 2018 data-taking period at $\sqrt{s} = 13$ TeV”, CMS Physics Analysis Summary CMS-PAS-LUM-18-002, 2019.
- [42] S. Frixione, P. Nason, and G. Ridolfi, “A Positive-weight next-to-leading-order Monte Carlo for heavy flavour hadroproduction”, *JHEP* **09** (2007) 126, doi:10.1088/1126-6708/2007/09/126, arXiv:0707.3088.
- [43] S. Alioli, P. Nason, C. Oleari, and E. Re, “A general framework for implementing NLO calculations in shower Monte Carlo programs: the POWHEG BOX”, *JHEP* **06** (2010) 043, doi:10.1007/JHEP06(2010)043, arXiv:1002.2581.
- [44] J. Alwall et al., “The automated computation of tree-level and next-to-leading order differential cross sections, and their matching to parton shower simulations”, *JHEP* **07** (2014) 079, doi:10.1007/JHEP07(2014)079, arXiv:1405.0301.
- [45] T. Sjöstrand et al., “An introduction to PYTHIA 8.2”, *Comput. Phys. Commun.* **191** (2015) 159, doi:10.1016/j.cpc.2015.01.024, arXiv:1410.3012.
- [46] CMS Collaboration, “Extraction and validation of a new set of CMS PYTHIA8 tunes from underlying-event measurements”, *Eur. Phys. J. C* **80** (2020) 4, doi:10.1140/epjc/s10052-019-7499-4, arXiv:1903.12179.
- [47] NNPDF Collaboration, “Parton distributions for the LHC Run II”, *JHEP* **04** (2015) 040, doi:10.1007/JHEP04(2015)040, arXiv:1410.8849.
- [48] CMS Collaboration, “Measurement of differential $t\bar{t}$ production cross sections in the full kinematic range using lepton+jets events from proton-proton collisions at $\sqrt{s} = 13$ TeV”, *Phys. Rev. D* **104** (2021) 092013, doi:10.1103/PhysRevD.104.092013, arXiv:2108.02803.
- [49] CMS Collaboration, “Search for $t\bar{t}$ resonances in highly-boosted lepton+jets and fully hadronic final states in proton-proton collisions at 13 TeV”, *JHEP* **07** (2017) 001, doi:10.1007/JHEP07(2017)001, arXiv:1704.03366.
- [50] CMS Collaboration, “Measurement of the top quark polarization and spin correlations using dilepton final states in proton-proton collisions at 13 TeV”, *Phys. Rev. D* **100** (2019) 072002, doi:10.1103/physrevd.100.072002, arXiv:1907.03729.
- [51] CMS Collaboration, “Measurement of the inelastic proton-proton cross section at $\sqrt{s} = 13$ TeV”, *JHEP* **07** (2018) 161, doi:10.1007/JHEP07(2018)161, arXiv:1802.02613.
- [52] CMS Collaboration, “Performance of the DeepJet b tagging algorithm using 41.9 fb^{-1} of data from proton-proton collisions at 13 TeV with the Phase 1 CMS detector”, CMS Detector Performance Report CMS-DP-2018-058, 2018.
- [53] J. Butterworth et al., “PDF4LHC recommendations for LHC Run II”, *J. Phys. G* **43** (2016) 023001, doi:10.1088/0954-3899/43/2/023001, arXiv:1510.03865.
- [54] R. J. Barlow and C. Beeston, “Fitting using finite Monte Carlo samples”, *Comput. Phys. Commun.* **77** (1993) 219, doi:10.1016/0010-4655(93)90005-W.